Int. J. Heat Mass Transfer. Vol. 36, No. 12, pp. 3119–3134, 1993
Printed in Great Britain

0017–9310/93 $6.00 + 0.00

Mixed convection in an inclined channel with a discrete heat source

C. Y. CHOI and A. ORTEGA
Department of Aerospace and Mechanical Engineering, The University of Arizona, Tucson, AZ 85721, U.S.A.

(*Received* 3 *June* 1992 *and in final form* 18 *November* 1992)

Abstract—The effects of laminar forced flow on buoyancy-induced natural convection cells throughout the regions of natural, mixed, and forced convection have been numerically investigated for a parallel planes channel with a discrete heat source. Emphasis is placed on the influence of the inlet flow velocity and the inclination angle of the channel, and the local buoyancy induced by the discrete source. The results indicate that the overall Nusselt number of the source strongly depends on the inclination angle (γ) in the natural and mixed convection regimes when $\gamma > 45°$. On the other hand, the changes in Nu and $\theta_{s,max}$ are negligible when the channel is from 0 to 45°, i.e. there is no significant penalty in heat transfer due to the inclination of the channel up to $\gamma = 45°$. As Gr increases at a fixed Re, the entrainment of the air from the downstream exit is observed for the case of aiding flow.

INTRODUCTION

WITH THE knowledge accumulated from previous studies on natural or forced convection in vertical and horizontal channels, considerable attention has recently turned to mixed convection problems because of a number of practical applications including cooling of electronic equipment and devices. As circuit densities increase at a rate of 30% per year, the heat flux or thermal dissipation per unit area continues to multiply [1]. Currently, natural convection and low Reynolds number forced convection heat transfer are useful for simple component power levels of the order of 1–5 W total, with a maximum chip junction temperature of 100°C or so. In a channel with a pressure-driven external flow, the increasingly high heat flux from electronic modules heightens the possibility of complex flows due to the buoyancy effects, which have been largely ignored in the past. It is important therefore to understand the interaction between buoyancy-induced flow and pressure-driven external flow, and the corresponding heat transfer characteristics in a channel.

Natural convection cooling of electronic equipment continues to be an important thermal control mechanism in applications such as telecommunications electronics, in which long time reliability is an overriding design criterion, and consumer electronics in which acoustic noise is undesirable. One of the challenges of passive cooling is enhancement of the relatively low heat transfer coefficient. It is well known that even modest increases in through-flow air velocity can double or triple the heat transfer coefficient from a discrete component, for example one on a vertically oriented PCB [2]. In typical passive cooling applications densely packed vertical boards are oriented in horizontal shelves or 'buckets' as shown in Fig. 1(a). There are competing mechanisms that determine the overall thermal performance. The overall induced mass flow rate scales with the overall cabinet height [1], but so too does the maximum card temperature, occurring roughly at the topmost card. A reduction in the maximum temperature can be achieved by card-staggering (as shown in Fig. 1(b)) which has been previously investigated [1]. With the increasing card-level power density system packaging alternatives are sought for enhanced thermal management with fixed maximum component temperature. One potential packaging alternative is the use of board inclination as illustrated in Fig. 1(c). We hypothesize that it may be possible to obtain substantial buoyant lift and therefore mass flow with reduced maximum card temperature.

A search of the literature revealed little substantive information on the effects of inclination in the proposed geometry, especially in mapping regions of heat transfer enhancement or degradation. The present work is an effort to elucidate the physics of inclined channels, with special attention to local buoyancy effects due to discrete heating and the attendant mixed convection when flow is induced into the channel by external means, whether it is by global chimney flow or fan-induced. We restrict our attention to a single channel with simplified boundary conditions as shown in Fig. 2.

PREVIOUS STUDIES

A complete review of the channel flow problem applied to electronics cooling is presented by Peterson and Ortega [1]. Kennedy and Zebib [3] presented results on the effects of free and forced laminar horizontal channel flow with a discrete heat source located on either the upper or the lower wall, and two heat sources on both walls. They suggested several guidelines for their thermal design of the electronic packages based on a comparison of the results. Incropera

NOMENCLATURE

B	gap width [m]
h	average heat transfer coefficient [W m^{-2} K^{-1}]
H	streamwise module length [m]
g	gravitational acceleration [m s^{-2}]
Gr	Grashof number, $g\beta qH^4/kv^2$
L	channel length [m]
Nu	overall Nusselt number, equation (8)
p	pressure [Pa]
P	dimensionless pressure, $p/\rho V_0^2$
Pr	Prandtl number
q	source heat flux [W m^{-2}]
Re	Reynolds number, V_0H/μ
t	time [s]
T	temperature [°C]
u, v	x- and y-direction velocities [m s^{-1}]
U, V	x- and y-direction dimensionless velocities, u/V_0 and v/V_0
x, y	dimensional coordinates [m]
X, Y	x- and y-direction dimensionless coordinates, x/H and y/H.

Greek symbols

β	coefficient of thermal expansion [°C^{-1}]
γ	angle of inclination from vertical [°]
θ	dimensionless temperature, $(T-T_c)/(qH/k)$
μ	dynamic viscosity [kg m^{-1} s^{-1}]
ν	kinematic viscosity, μ/ρ [m^2 s^{-1}]
ρ	density of fluid [kg m^{-3}]
τ	dimensionless time, V_0t/H
Φ	convergence criterion, equation (7).

Subscripts

c	cold wall
o	inlet
max	maximum
s	module surface.

Superscripts

N	number of iterations.

and co-workers have performed a series of numerical and experimental studies in a rectangular horizontal channel. Mixed convection in the entrance region was extensively discussed [4–6]. Conjugate mixed convection from a discrete thermal source or multiple sources in a rectangular cavity was investigated by Papanicolaou and Jaluria [7, 8]. They observed that the location of the source on the right vertical wall is the most favorable in terms of cooling, and that oscillatory flow and thermal fields may develop in the enclosure depending on the relative location of the components at high inputs by the components.

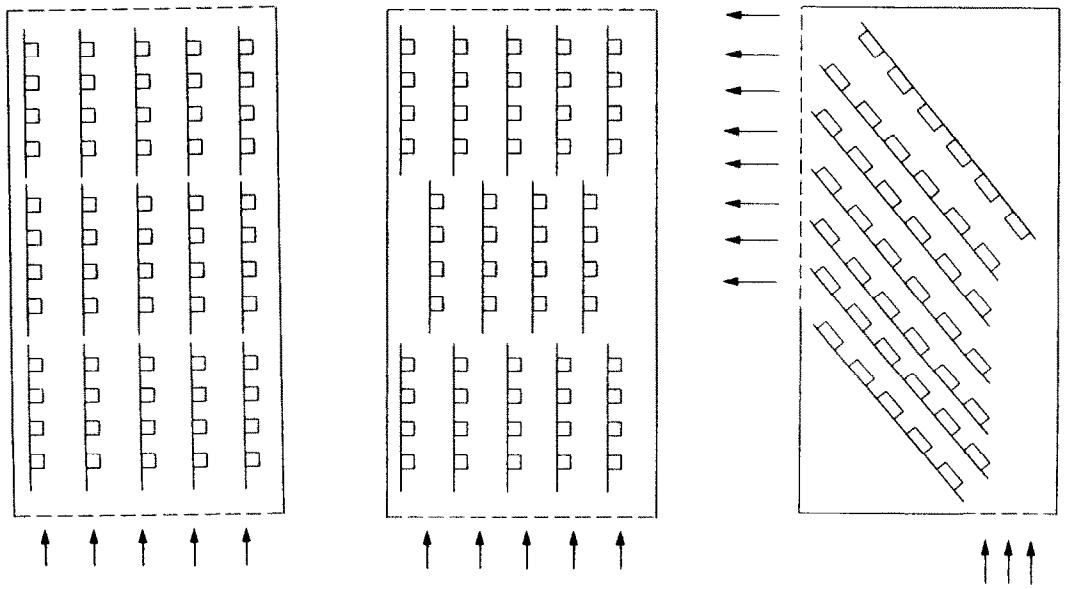

FIG. 1. Printed circuit boards in a cabinet, (a) in-line boards, (b) staggered boards, (c) inclined boards.

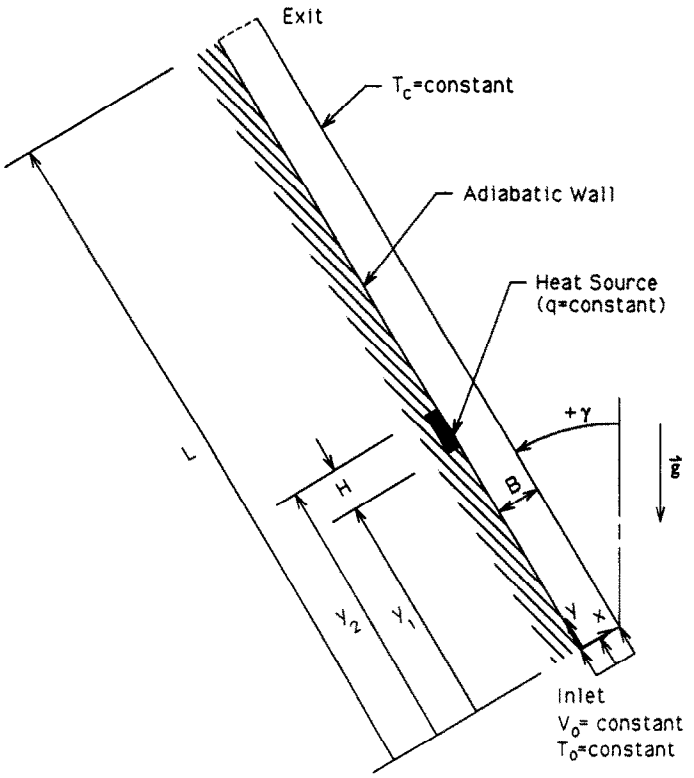

FIG. 2. The geometry of the channel with a flush-mounted module.

In a vertical channel with a sudden expansion. Lin *et al.* [9] studied the influence of flow separation and recirculation on the performance of heat transfer devices. In particular, a flow reversal from the downstream section which occurs when the inlet flow rate is smaller than what could be achieved if the duct was operated in the natural convection flow mode has been discussed. Elpidorou *et al.* [10] investigated mixed convection in a vertical channel with a finite wall heat source, and their results revealed the fundamental nature of mixed convection in a vertical channel.

The effects of inclination angle on the flow and heat transfer characteristics under buoyancy-assisting flow conditions have been studied by Naito and Nagano [i 1] in the entrance region between parallel plates and Lin *et al.* [12] in a duct with a backward facing step. Both studies [11, 12] indicated that the inclination angle could play an important role in the velocity and temperature fields. A literature survey failed to reveal a complete investigation from natural to mixed to forced convection in an inclined channel including buoyancy-opposing flow conditions. The present study investigates the effects of both buoyancy-assisting and opposing flows in a single inclined channel with a discrete heat source. Horizontal channels are also considered. Special attention is given to the maximum surface temperature on the module in addition to the overall heat transfer characteristics, because one of the most important objectives of thermal control in electronic packages is to maintain the component temperature below the manufacturer's maximum specified operating temperature.

FORMULATION AND NUMERICAL PROCEDURE

The geometry considered is an inclined channel in which a constant-flux heat source of finite length is located on one side, while the opposite wall is isothermal as shown in Fig. 2. The module size equals the channel gap ($H = B$), and a pressure-driven external flow is maintained through the channel. The module is flush-mounted and located from $y = 5H$ (y_1) to $y = 6H$ (y_2), and the total length of the channel is 15 times that of the module size ($L = 15H$). Depending upon the inclination angle, γ, the external flow can either aid or oppose the buoyancy force. In this study, we have considered three aiding ($\gamma = 0, 45$ and $-45°$), three opposing ($\gamma = 180$, 135 and $-135°$), and two horizontal ($\gamma = 90$ and $-90°$) cases. It is assumed that the inlet and the cold wall temperatures are the same, i.e. $T_o = T_c$. Using the Boussinesq approximation, the dimensionless governing equation for the laminar, two-dimensional flow are

$$\frac{\partial U}{\partial X} + \frac{\partial V}{\partial Y} = 0 \tag{1}$$

$$\frac{\partial U}{\partial \tau}+U\frac{\partial U}{\partial X}+V\frac{\partial U}{\partial Y}=-\frac{\partial P}{\partial X}+\frac{1}{Re}\left(\frac{\partial^2 U}{\partial X^2}+\frac{\partial^2 U}{\partial Y^2}\right)+\frac{Gr}{Re^2}\theta\sin\gamma \quad (2)$$

$$\frac{\partial V}{\partial \tau}+U\frac{\partial V}{\partial X}+V\frac{\partial V}{\partial Y}=-\frac{\partial P}{\partial Y}+\frac{1}{Re}\left(\frac{\partial^2 V}{\partial X^2}+\frac{\partial^2 V}{\partial Y^2}\right)+\frac{Gr}{Re^2}\theta\cos\gamma \quad (3)$$

$$\frac{\partial \theta}{\partial \tau}+U\frac{\partial \theta}{\partial X}+V\frac{\partial \theta}{\partial Y}=\frac{1}{Re\cdot Pr}\left(\frac{\partial^2 \theta}{\partial X^2}+\frac{\partial^2 \theta}{\partial Y^2}\right) \quad (4)$$

where Gr, Re, and coordinate variables are based on H, and the dimensionless velocities are based on the inlet velocity, V_0.

The corresponding boundary conditions at the walls are given as

$$U=V=0 \quad \text{at} \quad X=0 \text{ and } 1 \quad (5a)$$

$$\frac{\partial \theta}{\partial X}=0 \quad \text{at} \quad X=0, \quad 0<Y<\frac{Y_1}{H},$$

and

$$\frac{Y_2}{H}<Y<\frac{L}{H} \quad (5b)$$

$$\frac{\partial \theta}{\partial X}=-1 \quad \text{at} \quad X=0 \quad \text{and} \quad \frac{Y_1}{H}\leqslant Y\leqslant\frac{Y_2}{H} \quad (5c)$$

$$\theta=0 \quad \text{at} \quad X=1. \quad (5d)$$

The inlet and exit boundary conditions are given as

$$U=0, \quad V=1, \quad \text{and} \quad \theta=0 \quad \text{at} \quad Y=0 \quad (6a)$$

$$\frac{\partial U}{\partial Y}=0, \quad \frac{\partial V}{\partial Y}=0, \quad \text{and} \quad \begin{cases} \dfrac{\partial \theta}{\partial Y}=0 & \text{if} \quad V\geqslant 0 \\ \theta=0 & \text{if} \quad V<0 \end{cases} \quad \text{at} \quad Y=\frac{L}{H} \quad (6b)$$

where the exit boundary conditions allow the flow reversal and the temperature of the entrained air is the same as the inlet temperature.

A finite-difference method (SIMPLER) has been adopted, and the numerical procedure is well described in ref. [13]. The code was validated by solving the benchmark problem of natural convection in a square enclosure, and results were compared with those presented by de Vahl Davis and Jones [14]. The comparison shows that the overall Nusselt numbers at the wall computed with our code were within 2% of the benchmark solutions in ref. [15] for the four Rayleigh numbers in the range 10^3–10^6. After a series of test runs, the convergence criteria for the steady state were defined as

$$|\Phi^{N+1}-\Phi^N|<10^{-4} \quad (7)$$

where N and Φ, respectively, represent the number of iterations and the dependent variables, i.e. V, U and θ. No significant improvement in the Nusselt number was observed for tighter convergence criteria. Five uniform and two non-uniform meshes were tested, and a 16×151 uniform grid was selected for the present calculations. The finer uniform mesh, 21×201, changed the heat transfer results very little (e.g. less than 1% when $Gr=10^4$ and $Re=1$). Two non-uniform meshes (11×101 and 16×151) were tested and the corresponding results showed slower convergence rates, although we found that non-uniform meshes noticeably improve the convergence rates for natural convection problems in enclosures including the benchmark case with the same code. A similar test result with the SIMPLER scheme was recently reported by Lin *et al.* [15].

Without the transient terms in equations (2)–(4), steady state solutions were obtained for most of the cases. In general, the relaxation parameters were 0.7 for the dimensionless velocities and 0.9 for the dimensionless temperature, and the typical overall number of iterations to reach steady state criteria was about 5000. For some opposing cases at $Gr=10^5$, it was difficult to achieve converged solutions even by using extremely low relaxation parameters of 0.1 or less. The flow patterns exhibit the formation of the secondary recirculating cells which may trigger the instability of the flow in the channel. Therefore, experiments would show unsteady, three-dimensional flows, if not outright turbulence. The false transient method was tested and adopted for those cases, and we were able to overcome the difficulty of numerical convergence and instability with small time steps ($10^{-4}\leqslant\tau\leqslant 10^5$). The overall number of iterations required was as high as 20000 in order to satisfy the convergence criteria. When the time step was higher than 10^{-3}, either divergence or oscillation in the overall Nusselt number and other dimensionless parameters was observed. An overall energy balance was used as an additional check on the accuracy of the result of each run. The difference between the energy input through the module and the energy loss through the exit, inlet, and cold wall ranged from 2–3% for most cases, while the difference reached as high as 10% for some opposing cases when $Gr=10^5$. Computations were performed on the CONVEX 240.

RESULTS AND DISCUSSION

Numerical results were obtained for $Pr=0.71$, and $0.1\leqslant Re\leqslant 500$, respectively. The results cover natural to mixed to forced convection for $Gr=10^3$, 10^4 and 10^5 at various inclination angles. It may be instructive to relate the dimensionless parameters to some real values. For $H=1$ cm and $L=15$ cm, as an example, the ranges of the velocity and the heat flux are 0.016 cm s$^{-1}\leqslant V_0\leqslant$ 78.4 cm s^{-1} and 0.002 W cm$^{-2}\leqslant q\leqslant$ 0.2 W cm^{-2}. Other important dimensionless parameters for the present study are the angle of inclination (γ) and the overall Nusselt number (Nu).

Here, the overall Nusselt number is defined as

$$Nu = \int_{Y_1/H}^{Y_2/H} \left[\frac{1}{\bar{\theta}}\right]_{X=0} \mathrm{d}Y. \tag{8}$$

The maximum dimensionless temperature on the module ($\theta_{s,max}$) is chosen as an additional parameter to be carefully examined.

Figure 3 shows the effects of channel orientation on the recirculating flow pattern at $Re = 1$ and $Gr = 10^3$. A recirculation cell is observed due to the local buoyancy for each aiding and opposing case, while a bicellular flow pattern is observed for the horizontal channel cases. The recirculating motions are possible because the opposite wall acts as a heat sink. It is clear that the external flow follows the rotational directions of the natural convection cells for all cases. As a result, the cells are consistently located near the cold wall for aiding flow and near the module for opposing flow. Considering both aiding and opposing mixed convection in a vertical porous annulus with a discrete heat source, Choi and Kulacki [16] numerically demonstrated the same flow patterns, and they investigated the effects of the location of the recirculating cell on the heat transfer results both numerically and experimentally.

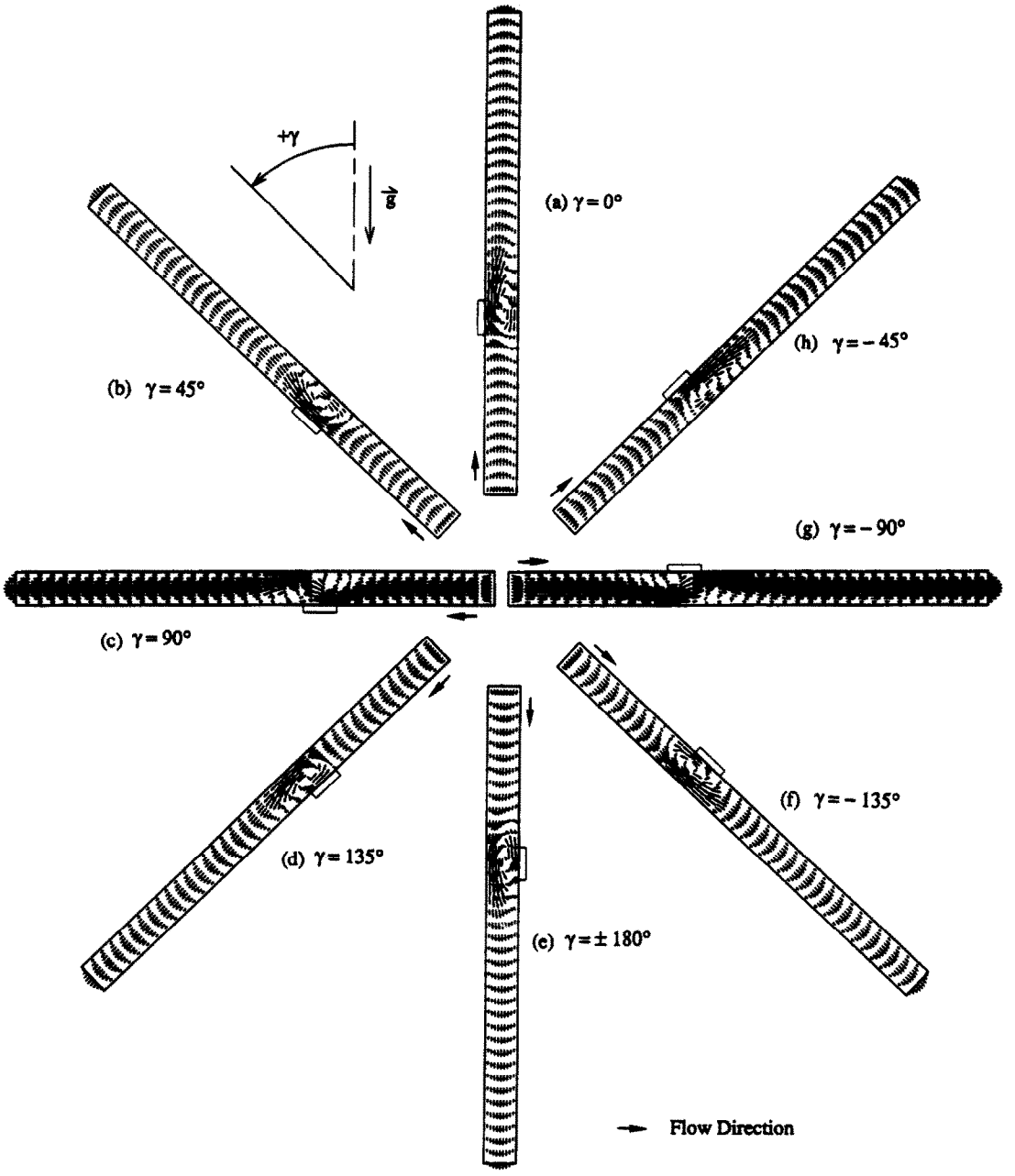

FIG. 3. Calculated streamlines at various orientations when $Gr = 10^3$, $Re = 1$.

The effects of aiding ($\gamma = 45°$) and opposing ($\gamma = -135°$) imposed flows on buoyancy-induced convection are visualized in Fig. 4 at $Gr = 10^4$. When the Peclet number is small (Figs. 4(a) and (d)), flow and temperature fields retain the major characteristics of natural convection. With the heat source located on the left side, the rotational direction of the recirculating cell is clockwise for $\gamma = -45°$. Due to the rotational direction of the cell, the external flow pushes the recirculating cell toward the cold wall as the Peclet number increases, while the flow directly contacts the heating module. For opposing flows, on the other hand, the downward external flow follows the counterclockwise recirculating cell and is swept toward the cold wall. Consequently, the natural convection cell is pushed toward the heat source as shown

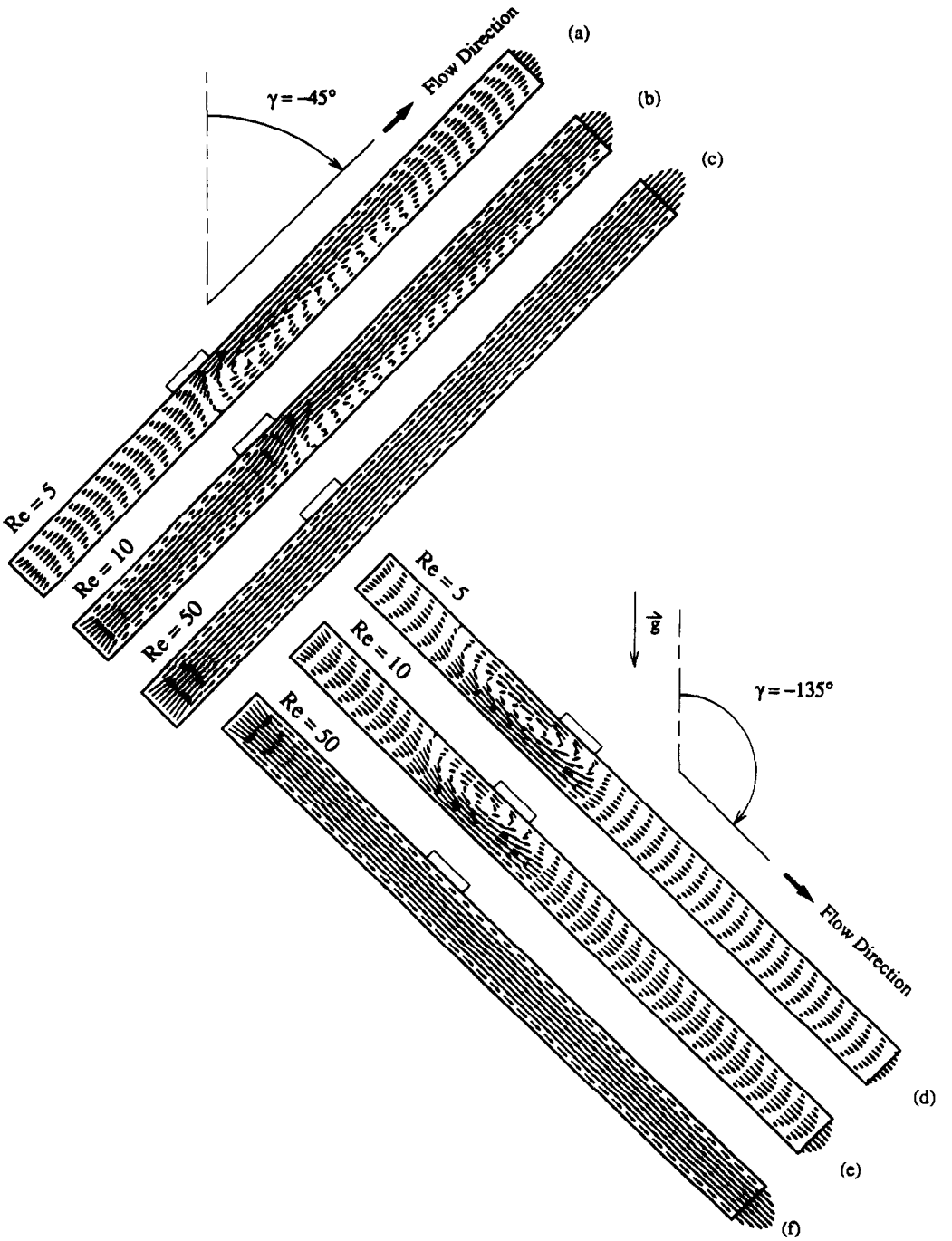

FIG. 4. Changes in flow fields with the increase of Re for aiding (a)–(c) and opposing (d)–(f) flows for $Gr = 10^4$.

in Figs. 4(d) and (e). Choi and Kulacki [16] reported that such a 'trapped' recirculating cell near the heat source raises the overall temperature of the heating surface, and the reduction in the heat transfer coefficient is significant in a vertical porous annulus. As the Peclet number further increases, the recirculating cells gradually disappear, and the channel angle becomes an insignificant factor on fluid flow and heat transfer in the channel.

The effect of module location in a horizontal channel is presented in Fig. 5. When the heat source is located at the bottom of the channel, i.e. $\gamma = 90°$, the sizes of the recirculating cells are smaller than those in which the heat source is located at the top ($\gamma = -90°$). However, based on the maximum vertical velocity for each case, the recirculating cells of the bottom-heated case ($V_{max} = 14.52$ at $Re = 1$) are much stronger than those of the top-heated case ($V_{max} = 6.38$ at $Re = 1$). As the Peclet number increases, the external flow suppresses the relatively weak recirculating cells for

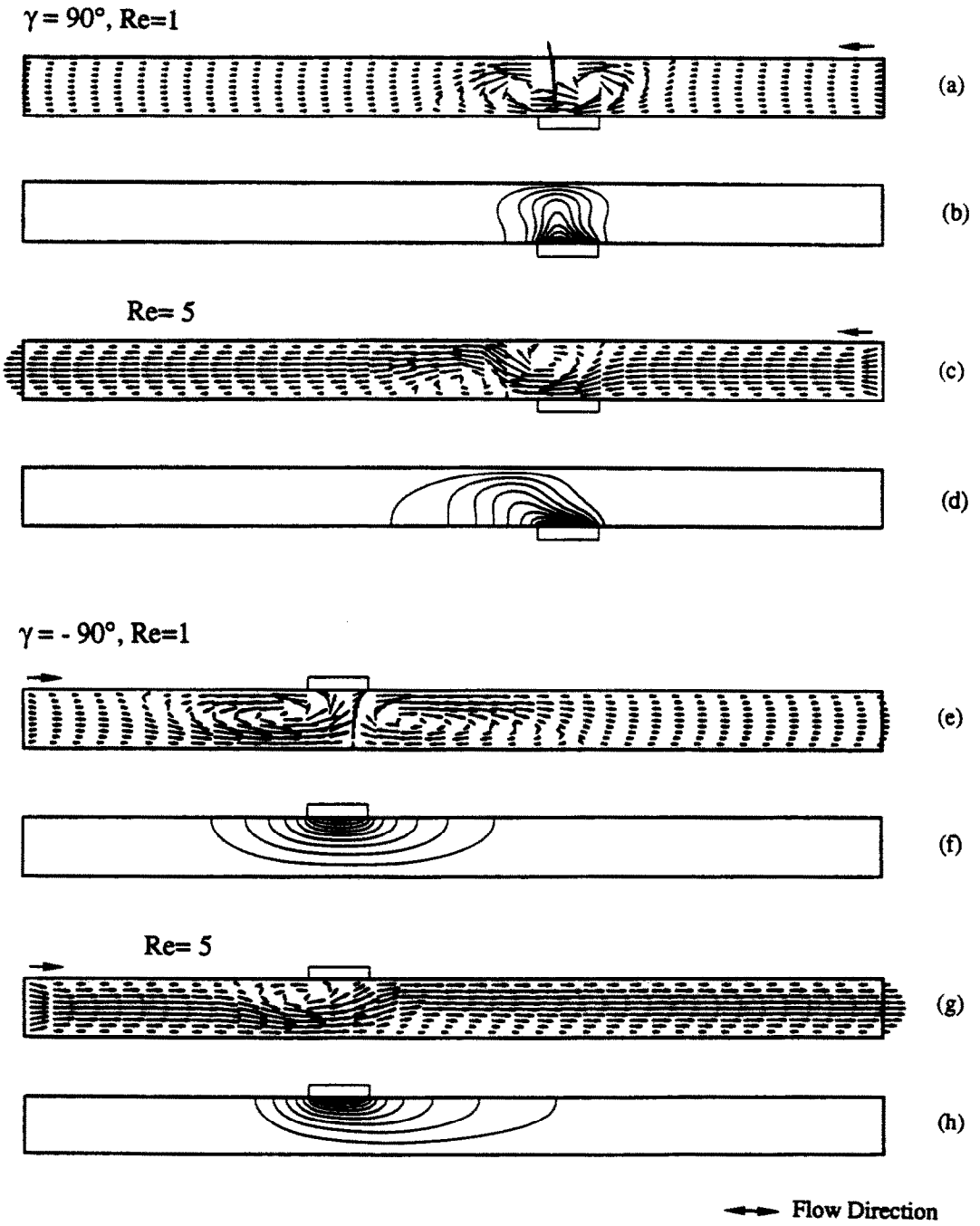

FIG. 5. The importance of the location of the module in a horizontal channel at low Re for $Gr = 10^4$.

$\gamma = -90°$ at low Re. Figure 5(g) shows that one of the cells nearly disappears due to the external flow, while Fig. 5(c) shows that both cells are still active at the same Peclet number ($Pe = 5$). It is also interesting to observe that the remaining cell in Fig. 5(g) is trapped near the heating surface, and such a flow pattern delays direct contact between the cold external flow and the heated surface. As a result, the maximum dimensionless surface temperatures for $\gamma = -90°$ are higher than those for $\gamma = 90°$; i.e. $\theta_{max} = 0.41$ at $Re = 1$ and 0.37 at $Re = 5$ for $\gamma = 90°$, while $\theta_{max} = 0.49$ at $Re = 1$ and 0.47 at $Re = 5$ for $\gamma = -90°$, respectively.

Figures 6(a)–(j) demonstrate the flow development in a horizontal and bottom-heated channel ($\gamma = 90°$). In the natural convection regime, the thermal plume

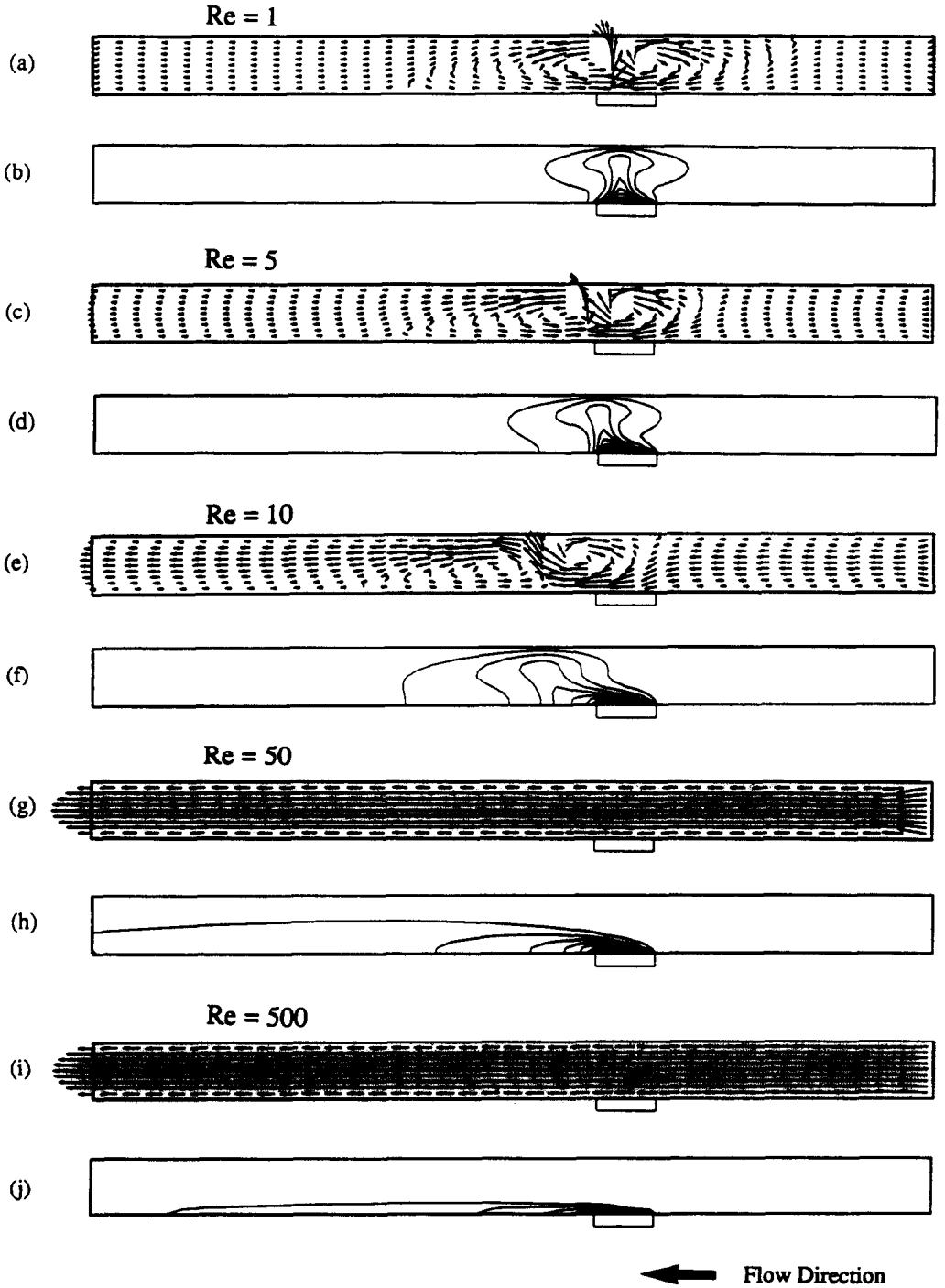

FIG. 6. Changes in flow and temperature fields with the increase of Re when $Gr = 10^5$, $\gamma = 90°$.

is nearly symmetric about the centerline of the module (Fig. 6(b)), and the plume shifts and stretches toward the downstream as the Peclet number increases. As the Peclet number increases further (Figs. 6(g)–(j)), the natural convection cells vanish and forced convection dominates the fluid flow pattern and the heat transfer process. The corresponding dimensionless temperature at the bottom wall and the heat flux through the cold wall are depicted in Figs. 7(a) and (b). The maximum dimensionless temperature decreases as Re increases (Fig. 7(a)). In the mixed convection region, the interaction between the natural convection cells and the pressure-driven external flow noticeably influences the surface temperature. For example, the highest surface temperature at $Y_2/H < Y < (Y_2/H+D/H)$ is obtained at $Re = 10$,

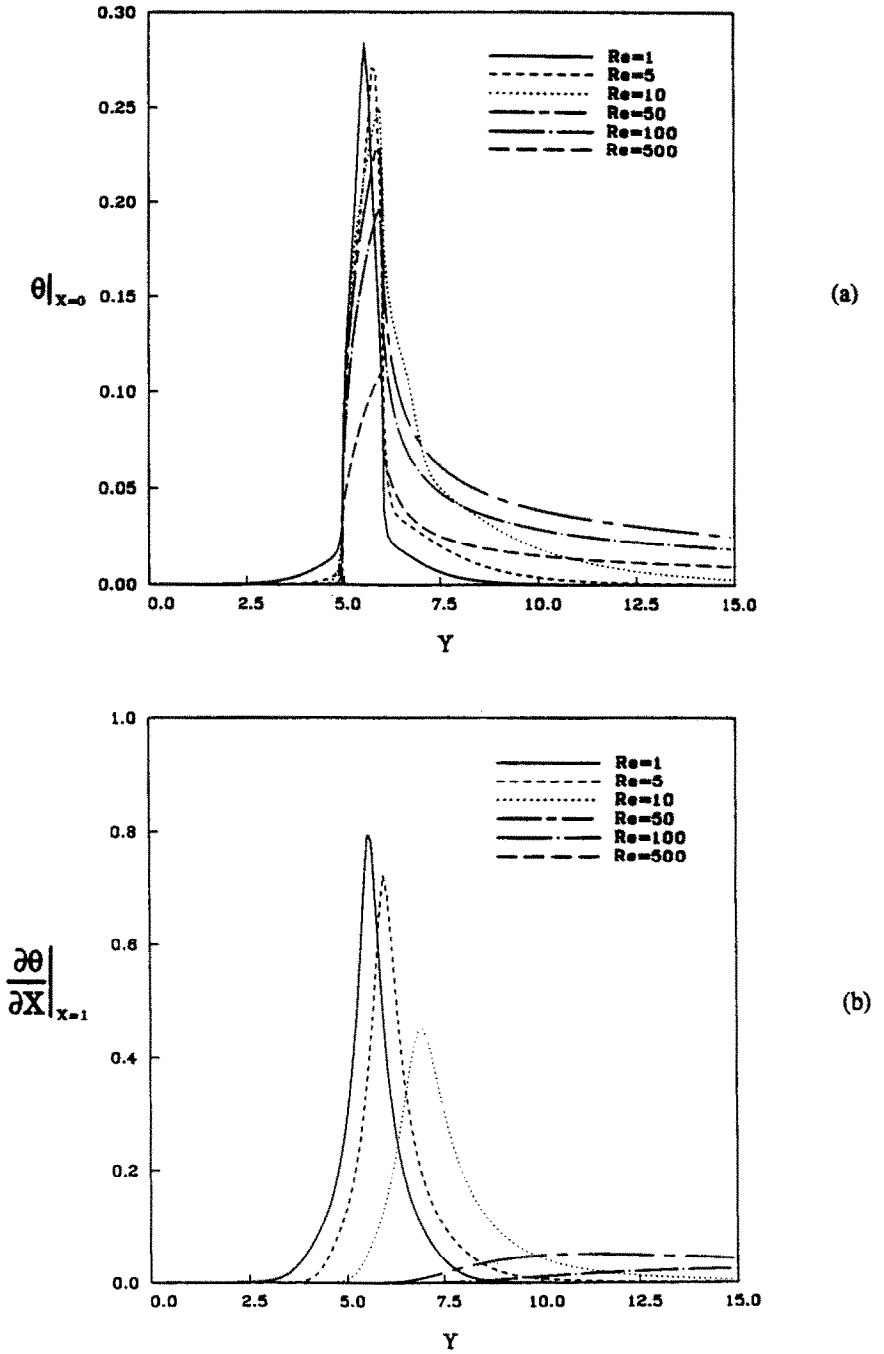

FIG. 7. Comparison of the dimensionless temperature on the bottom surface and the dimensionless heat flux through the cold wall at various Re when $Gr = 10^5$, $\gamma = 90°$.

since the external flow is heated by the module and driven by a strong recirculating cell attached to the cold wall toward the adiabatic region next to the module in the downstream. As shown in Fig. 7(b), the dimensionless heat flux through the cold wall dramatically decreases as Re increases. In particular, the heat flux is nearly zero for $Re = 500$, and the energy balance check shows that nearly 100% of the thermal energy from the source is convected out of the channel rather than conducted through the cold wall.

As mentioned earlier, flow reversal at the exit can occur when the inlet flow rate is restricted at high Grashof number. For the present study, all of the aiding cases (i.e. $\gamma = -45, 0, 45^\circ$) at $Gr = 10^5$ and at the low Reynolds number range ($Re \leqslant 10$) exhibit this phenomenon. Figures 8(a)–(h) present the devel-

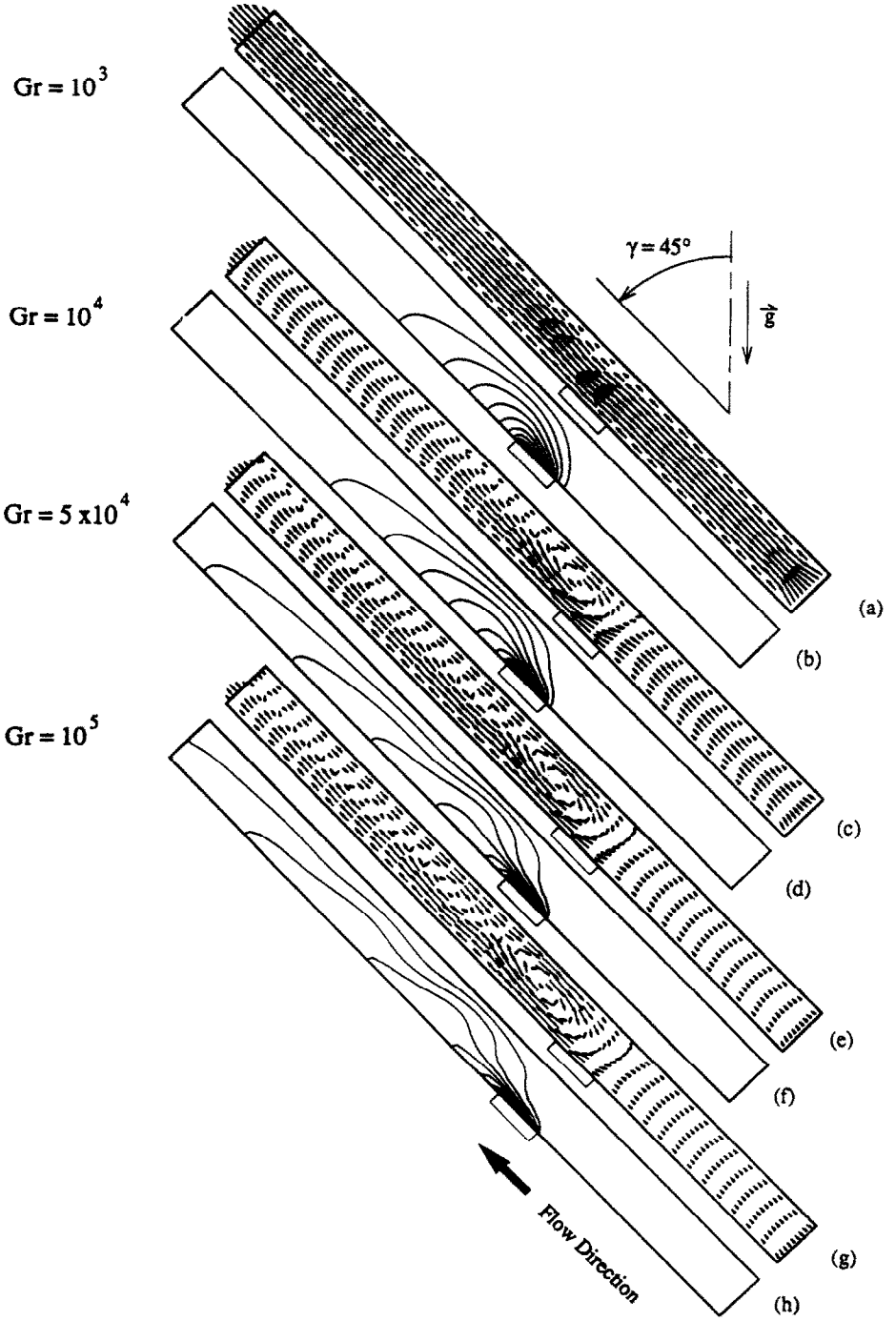

FIG. 8. Development of a reversed flow and secondary recirculating cells when $Re = 5$, $\gamma = 45^\circ$.

opment of a reversed flow at the exit section of the channel at $Re = 5$ and $\gamma = 45°$. As the Grashof number increases, the recirculating cell stretches to the exit section of the channel, and entrainment of air from the outside of the channel occurs. It is interesting to observe the formation of the secondary recirculating cells in Fig. 8(g), and that as a result of this formation, the corresponding isothermal lines are distorted as shown in Fig. 8(h). Considering the limit of zero inlet flow ($Re \to 0$), Lin *et al.* [9] suggested that the flow would start to exhibit a three-dimensional behavior, and possible transition to turbulent flow might follow. The present authors cautiously agree with their suggestion based on the observation of the developing secondary recirculating cells since those cells may trigger the instability of the flow in the channel. Experimental work is essential to verify this transition.

Based on the 'five percent deviation rule' suggested by Sparrow *et al.* [17], the natural, mixed, and forced convection regimes can be determined from Figs. 9(a)–(c). The figures indicate that the mixed convection regimes are approximately $1 < Re < 50$ for $Gr = 10^3$, $5 < Re < 100$ for $Gr = 10^4$, and $10 < Re < 500$ for $Gr = 10^5$. In the limit of natural convection, the data points scattered because of the channel orientation. The collapse of the data at high Re explains that the buoyancy effects—and thus the effects of orientation—diminish as forced convection dominates. The reduction in the Nusselt number in the mixed convection regime has been clearly shown in Figs. 9(b) and (c), mostly for opposing flows. This characteristic will be explained later in conjunction with the flow pattern.

The variations in $\theta_{s,max}$ and Nu due to the inclination of the channel are shown in Figs. 10–12. At $Gr = 10^3$ (Fig. 10), neither $\theta_{s,max}$ nor Nu are strongly dependent on γ at the natural and forced convection limits, while $\theta_{s,max}$ somewhat increases and Nu decreases at $\gamma = 180°$ in the mixed convection region. The explanation is that the natural convection cells at $Gr = 10^3$ are not strong enough to influence the flow and temperature fields in the natural convection regime; i.e. the heat transfer mode is rather close to conduction. As Gr increases (Figs. 11 and 12), however, the variations in $\theta_{s,max}$ and Nu are significant at the low Reynolds number range. In the natural and mixed convection regime, the most desirable situation in the cooling of the electronic module—the lowest $\theta_{s,max}$ and/or the highest overall Nusselt number—occurs when the angle of the channel is $0° < \gamma < 45°$, in general. For the application of the results of the present work, perhaps the most significant observation is that little or no penalty is associated with inclining the channel up to $\pm 45°$. Figures 11 and 12 also suggest that the cases as $\gamma = -90$ and 135° should be avoided at low Reynolds numbers. In the mixed convection regime, however, the channel angle for the highest $\theta_{s,max}$ varies depending upon Re and Gr. For example, when $Gr = 10^5$ as shown in Fig. 12, the worst cooling situations for the module occur at $\gamma = -90$ and 135°

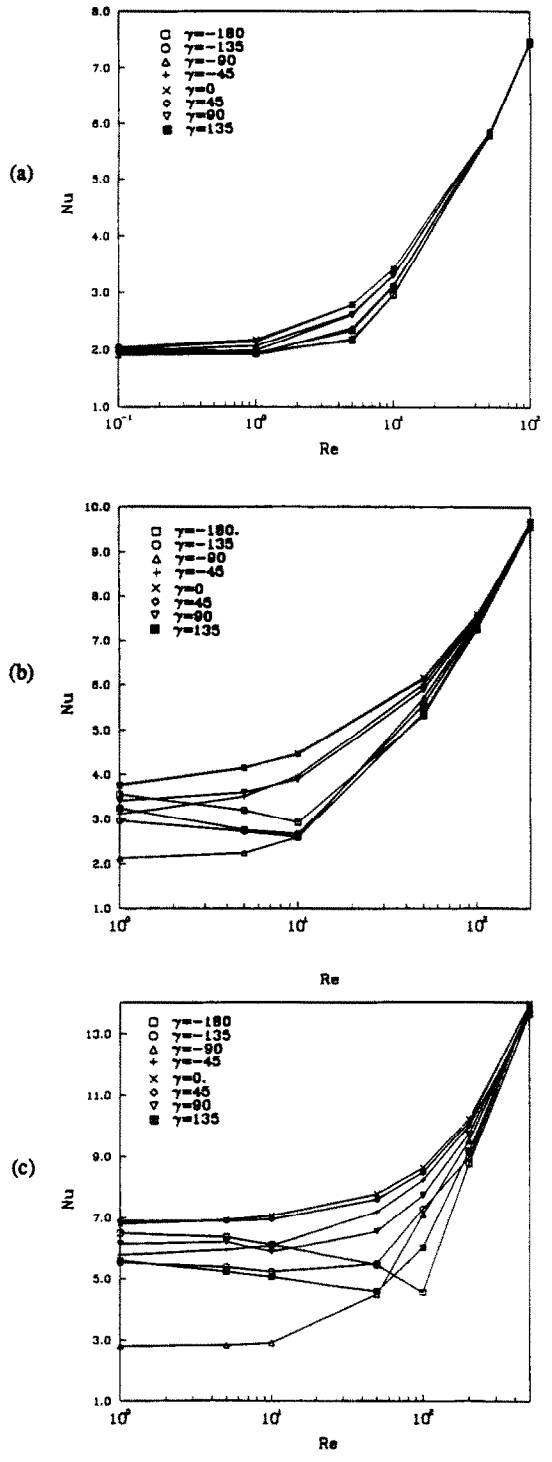

FIG. 9. Comparison of the overall Nusselt number at various values of Re at (a) $Gr = 10^3$, (b) $Gr = 10^4$, (c) $Gr = 10^5$.

for $Re = 50$, at $\gamma = -180$ and $-135°$ for $Re = 100$, and at $\gamma = -180$ for $Re = 200$, respectively. It is important to notice that the increase of Re does not necessarily decrease $\theta_{s,max}$ in the mixed convection regime for the opposing and the horizontal cases ($\gamma = 135$, 180, -135, and 90°). The influence of the

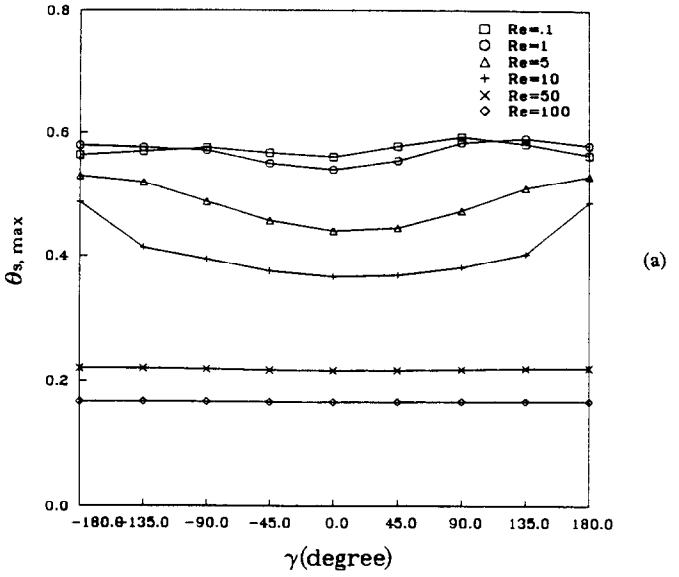

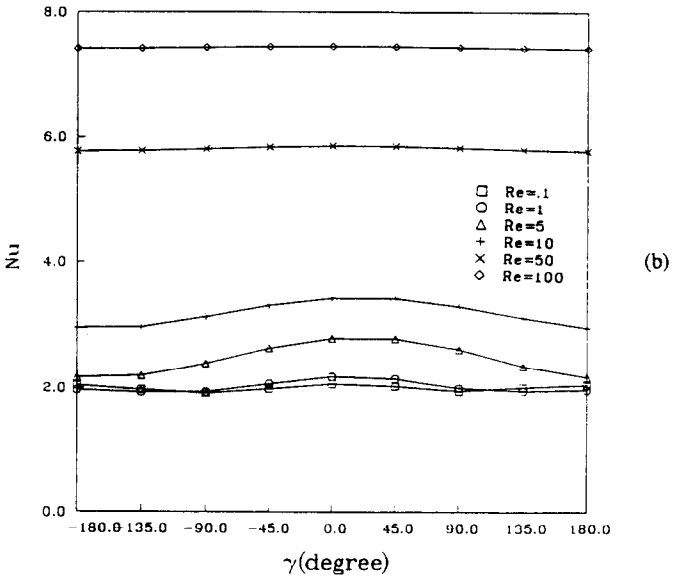

FIG. 10. Comparison of the maximum dimensionless temperature and the overall Nusselt number at various angles for $Gr = 10^3$.

channel angle disappears gradually as the Reynolds number increases. At this point, it may be interesting and instructive to see the same trends in terms of dimensional values. As an example, the maximum dimensional temperatures are listed in Table 1 at the various Reynolds numbers when $Gr = 10^4$, $T_c = 27°C$, $H = 1$ cm, and $L = 15$ cm.

Figures 13(a) and (b) show the results of $\theta_{s,max}$ and Nu as a function of Gr/Re^2 (known as 'the Richardson number') when the Grashof number is kept fixed at 10^5. The lowest $\theta_{s,max}$ and the highest Nusselt number occur at $\gamma = 0°$ and/or 45°. On the other hand, the highest $\theta_{s,max}$ and the lowest Nusselt number are obtained at the various orientation angles. Such a complexity is mainly due to the flow structure in the natural and mixed convection regime. It should be noted that these trends are true for the cases of $Gr = 10^3$ and 10^4 (the plots are omitted here). Figure 13(b) indicates that the mixed convection regime ranges approximately $5 \times 10^{-1} < Gr/Re^2 < 10^5$, and that the reduction of the Nusselt number, as briefly mentioned earlier, is shown in this region. When opposing flow is imposed in the mixed convection regime, a recirculating cell is placed next to the module

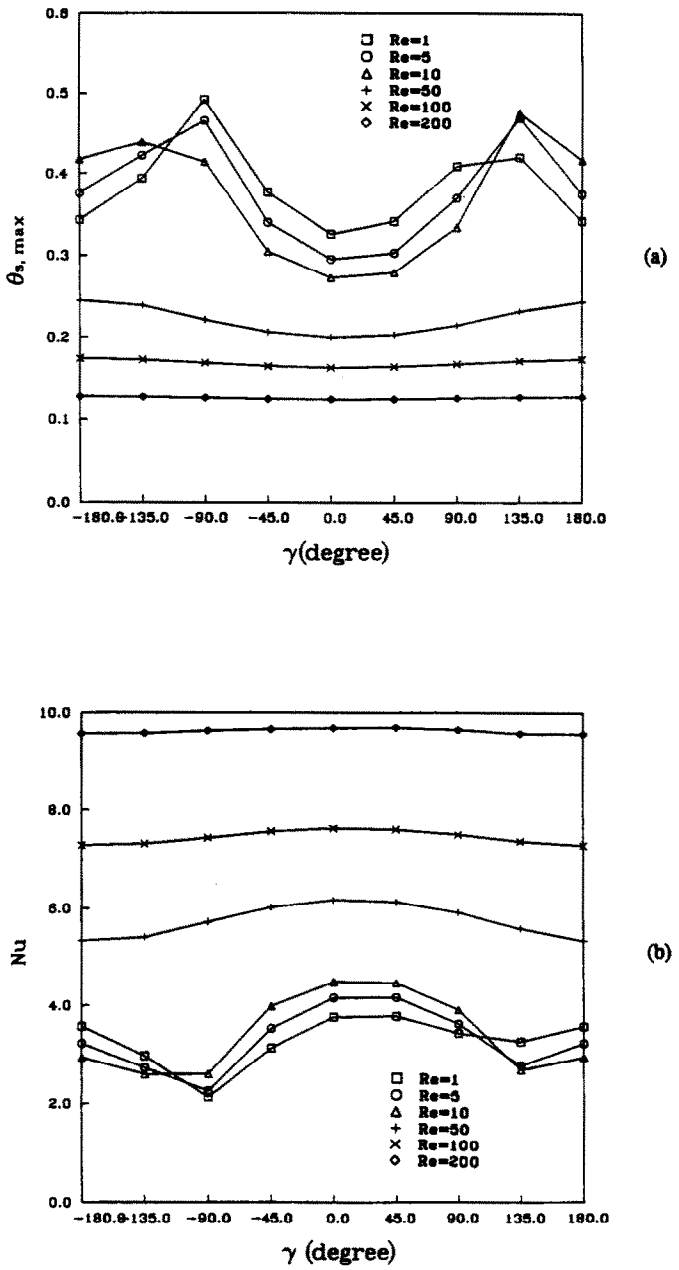

FIG. 11. Comparison of the maximum dimensionless temperature and the overall Nusselt number at various angles for $Gr = 10^4$.

as we observed in Figs. 3(d)–(f). The cell diverts the cold external flow from the heat source, while maintaining the relatively warm air inside. Such a flow structure inefficiently rejects the heat from the module and raises the surface temperature of the module. When the heating element is mounted on the top surface of the horizontal channel ($\gamma = -90°$), the strength of the convection cells is relatively weak in comparison with the cells of the bottom-heated case, hence, the heat transfer from the module is poor in the natural convection regime. As a result, the highest $\theta_{s,max}$ occurs at $\gamma = -90°$ approximately for $Gr/Re^2 > 5 \times 10^3$ (Fig. 13(b)). As Gr/Re^2 further decreases (or Re increases), $\theta_{s,max}$ decreases dramatically; i.e. the external flow sweeps away the tendency for the recirculating cells and quickly dominates the flow field as explained in conjuction with Fig. 5(g). For the horizontal channel with a module located at the bottom ($\gamma = 90°$), a slight reduction in Nu occurs as Gr/Re^2 decreases to 10^3 because the horizontal forced flow breaks up the active bicellular flow pattern and reduces the overall heat transfer coefficient until forced convection starts to dominate again.

From observation of Figs. 9–13, one can conclude

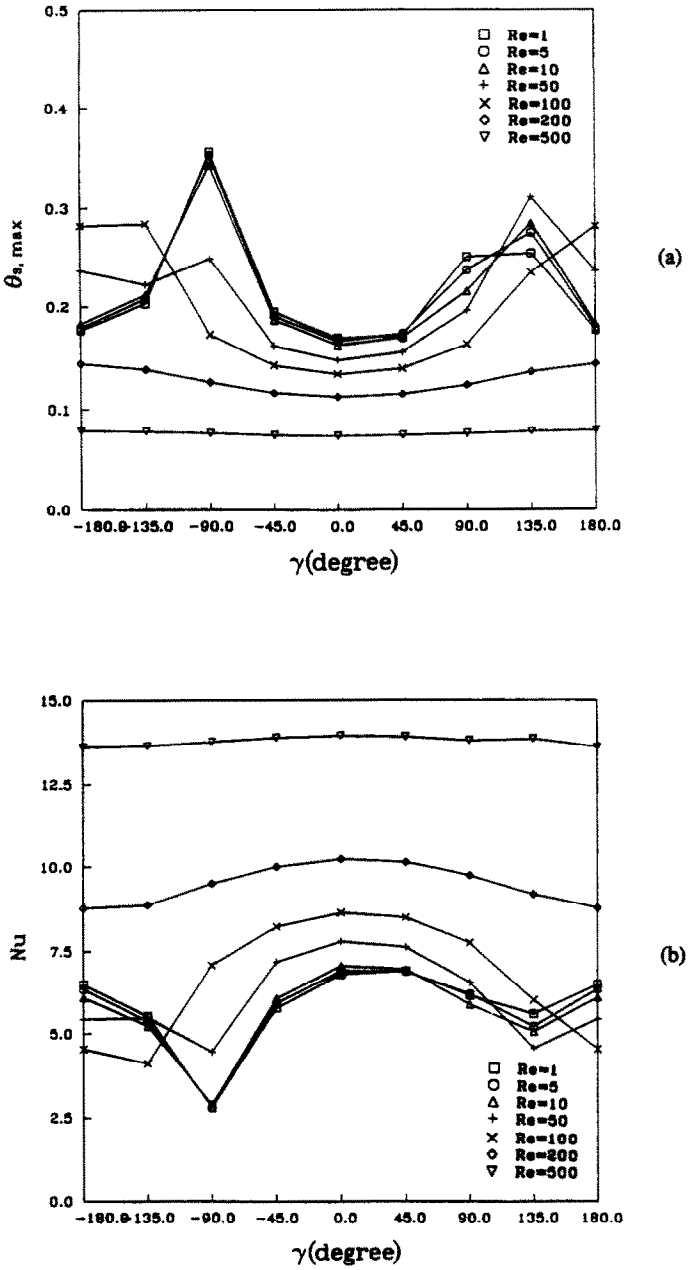

FIG. 12. Comparison of the maximum dimensionless temperature and the overall Nusselt number at various angles for $Gr = 10^5$.

that the best performance in heat transfer occurs when $\gamma = 0°$. From a system packaging point of view, it is also important to notice that the changes in Nu and $\theta_{s,max}$ are negligible when the channel is inclined from 0 to 45°, i.e. there is no significant penalty in heat transfer due to the inclination of the channel up to $\gamma = 45°$. We conclude that the practical use of inclined circuit boards in a cabinet may be possible. We also note here that further investigation of this potential geometric arrangement should consider effects of the overall height of a 'stack' of inclined boards.

A reversed flow from the downstream section of the channel has been observed for $\gamma = -45$, 0, and 45° when $Re \leqslant 10$ and $Gr = 10^5$. However, Figs. 9(c), 13(a) and (b) show that $\theta_{s,max}$ and Nu approach asymptotic values in the natural convection limit, and thus, no noticeable influence of the reversed flow is apparent. The authors believe that the additional buoyancy force due to the cold reversed flow occurs, while the same reversed flow keeps heated air from contacting the cold wall and suffocates the air flow from the downstream of the channel. Such a compensation may produce no apparent influence in the heat transfer coefficient, although the patterns of

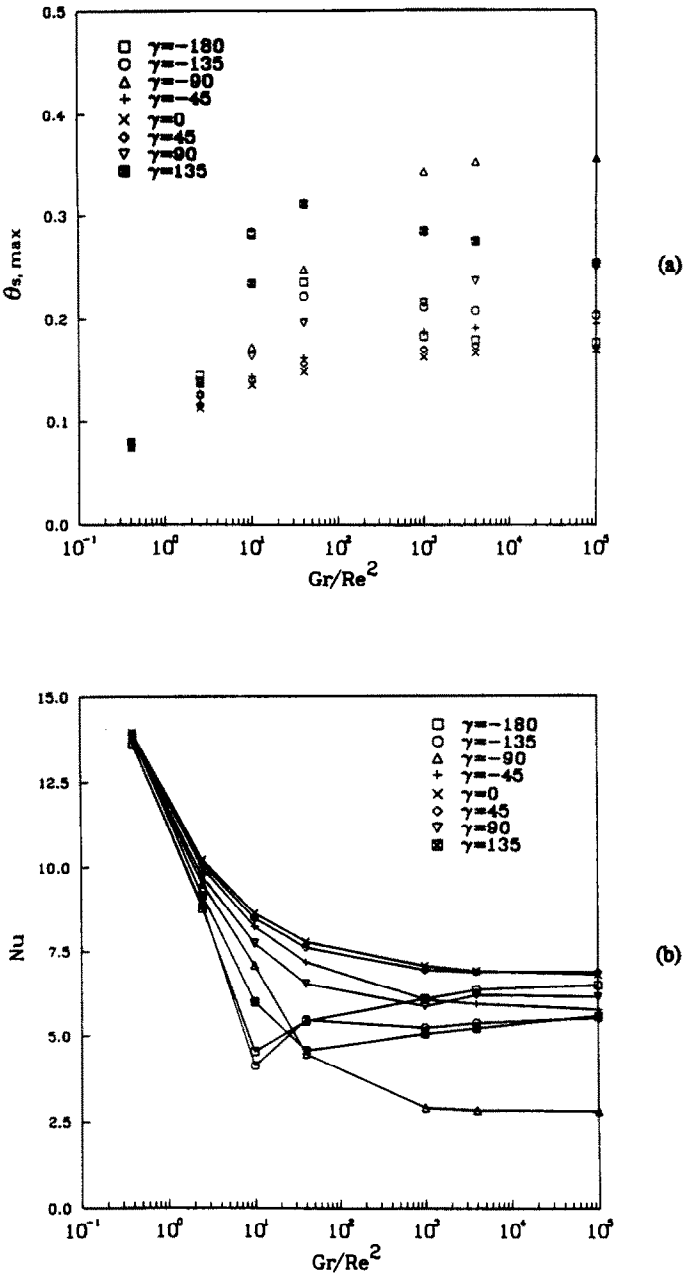

FIG. 13. (a) Variations in the maximum dimensionless temperature on the module surface, and (b) comparison of the overall Nusselt number at various Gr/Re^2 for $Gr = 10^5$.

downstream flow and isotherm are greatly changed as mentioned earlier. The heat transfer coefficient may be significantly influenced if the hydrodynamic instability and the three-dimensional and/or turbulent flow occur due to the flow reversal. Furthermore, the effect would be sensed on other components populating the surface.

CONCLUSIONS

The effects of the pressure-driven flow on the natural convection cells and the orientation of the channel have been investigated. Although a simple geometry has been considered, this study presents important fundamental aspects of mixed convection. The heat transfer results explain the importance of the channel orientation in the natural and mixed convection regime. For the opposing and horizontal cases in particular, the maximum surface temperature on the module does not always decrease as the external channel flow rate increases in the mixed convection region due to the interaction between convection cells and the external flow. A reversed flow has been observed and investigated at low *Re* and high *Gr*. The flow

Table 1. Maximum temperatures, T_{max}, at various velocities when $Gr = 10^4$, $T_c = 27°C$, $L = 15$ cm, and $H = 1$ cm

		T_{max}[°C]			
Re	V_o[cm/s]	$\gamma = 180°$	$\gamma = -90°$	$\gamma = 0°$	$\gamma = 90°$
1	0.16	51.8	61.7	50.0	55.9
10	1.57	56.4	56.2	46.3	50.2
50	7.84	44.3	42.6	41.2	42.2
200	31.36	35.9	35.8	35.8	35.8

reversal does not noticeably influence the heat transfer coefficient on the module, although the entrainment of air from the exit section changes the flow and temperature fields significantly. Such a flow development suggests a possibility for hydrodynamic instability and three-dimensional and/or turbulent flow patterns. The best performance in heat transfer has been observed when $\gamma = 0°$; however, no significant difference in heat transfer coefficient has been observed when $\gamma = 45°$. Therefore, the results shed some light on the practical use of inclined boards in a cabinet, and encourage further exploration.

REFERENCES

1. G. P. Peterson and A. Ortega, Thermal control of electronic equipment and devices, *Adv. Heat Transfer* **20,** 181–314 (1990).
2. R. J. Moffat and A. Ortega, Direct air-cooling of electronic components, *Advances in Thermal Modeling of Electronic Components and Systems*, Vol. 1, Chapter 3 (Bar-Cohen A. and Kraus A. D., Eds). Hemisphere, New York (1988).
3. K. J. Kennedy and A. Zebib, Combined free and forced convection between horizontal parallel planes: some case studies, *Int. J. Heat Mass Transfer* **26,** 471–474 (1983).
4. H. V. Mahaney, F. P. Incropera and S. Ramadhyani, Comparison of predicted and measured mixed convection heat transfer from an array of discrete source in a horizontal rectangular channel, *Int. J. Heat Mass Transfer* **33,** 1233–1245 (1990).
5. J. R. Maughan and F. P. Incropera, Regions of heat transfer enhancement for laminar mixed convection in a parallel plate channel, *Int. J. Heat Mass Transfer* **33,** 555–570 (1990).
6. J. R. Maughan and F. P. Incropera, Use of vortex generators and ribs for heat transfer enhancement at the top surface of a uniformly heated horizontal channel with mixed convection flow, *ASME J. Heat Transfer* TN, **113,** 504–507 (1991).
7. E. Papanicolaou and Y. Jaluria, Conjugated mixed convection from thermal sources in a rectangular cavity, *Proc. ASME Winter Annual Meeting* **HTD-157,** 29–40 (1990).
8. E. Papanicolaou and Y. Jaluria, Forced and mixed convective cooling of multiple electronic components in an enclosure, *Proc. ASME/A.I.Ch.E. natl Conf.* **HTD-171,** 29–37 (1991).
9. J. T. Lin, B. F. Armaly and T. S. Chen, Mixed convection in buoyancy-assisting, vertical backward-facing step flows, *Int. J. Heat Mass Transfer* **33,** 2121–2132 (1990).
10. D. Elpidorou, V. Prasad and V. Modi, Convection in a vertical channel with a finite wall heat source, *Int. J. Heat Mass Transfer* **34,** 573–578 (1991).
11. E. Naito and Y. Nagano, Combined forced and free upward-flow convection in the entrance region between inclined parallel plates, *ASME J. Heat Transfer*, **111,** 675–682 (1989).
12. J. T. Lin, B. F. Armaly and T. S. Chen, Mixed convection heat transfer in inclined backward-facing step flows. *Int. J. Heat Mass Transfer* **34,** 1568–1571 (1991).
13. S. V. Patankar, *Numerical Heat Transfer and Fluid Flow*. McGraw-Hill, New York (1981).
14. G. de Vahl Davis and I. P. Jones, Natural convection of air in a square cavity: a benchmark numerical solution. *Int. J. Numer. Meth. Fluids* **3,** 227–264 (1983).
15. Y. T. Lin, M. Choi and R. Grief, A three-dimensional analysis of the flow and heat transfer for the modified chemical vapor deposition process including buoyancy, variable properties, and tube rotation, *ASME J. Heat Transfer* **113,** 400–406 (1991).
16. C. Y. Choi and F. A. Kulacki, Mixed convection through vertical porous annuli locally heated from inner cylinder, *ASME J. Heat Transfer* **114,** 143–151 (1992).
17. E. M. Sparrow, R. Eichhorn and J. L. Gregg, Combined forced and free convection in a boundary layer, *Phys. Fluids* **2,** 319–329 (1959).